ENCIT 2018

ABCM Associação Brasileira de Engenharia e Ciências Mecânicas

17th Brazilian Congress of Thermal Sciences and Engineering
November 25th-28th, 2018, Águas de Lindóia, SP, Brazil

ENCIT-2018-0143
EXPERIMENTAL STUDY OF THE INFLUENCE OF THE SWIRL NUMBER ON LEAN PREMIXED COMBUSTION REGIMES

Letícia Carneiro Piton, Gabriela Senra Pessanha Rios Nobrega, Luís Fernando Figueira da Silva
Pontifícia Universidade Católica do Rio de Janeiro, Department of Mechanical Engineering, Rio de Janeiro, Brazil.
leticiacpiton@gmail.com, gabi.senra@hotmail.com, luisfer@puc-rio.br

Philippe Scouflaire, Nasser Darabiha
Laboratoire EM2C, CNRS, CentraleSupélec, Université Paris-Saclay, Gif-sur-Yvette, France.
philippe.scouflaire@cnrs.fr, nasser.darabiha@centralesupelec.fr

Abstract. *Lean premixed turbulent swirling combustion is known for significantly reducing pollutants emissions, when compared to non-premixed turbulent flames. Characterizing the swirl number influence is therefore essential to comparing different combustion chamber operational regimes. The present study is devoted to the experimental characterization of a new family of swirlers currently being developed in a partnership between PUC-Rio and EM2C/CNRS laboratory at CentraleSupelec. The associated combustion process is found to exhibit different flame topologies, or combustion regimes, which are functions of the mixture equivalence ratio and flow rate. The flame topologies and the boundaries between the observed combustion regimes are evidenced by means of OH^* chemiluminescence and overall flame chemiluminescence.*

Keywords: *experimental study, swirling flows, flame topology, premixed turbulent flames*

1. INTRODUCTION

Lean premixed turbulent combustion is known for significantly reducing pollutants emissions when compared to non-premixed turbulent flames. These premixed flames are often considered in swirling combustion chamber configurations, where the swirl number influence has been shown to be paramount on turbulent flame topologies, blow-off or flashback limits and on the acoustic stability properties (Huang and Yang, 2009; Candel *et al.*, 2014; Chterev *et al.*, 2014). Characterizing the swirl number influence is therefore essential to comparing different combustion chamber operational regimes. Such comparison is particularly relevant when novel swirler designs are sought, which is the case of the present endeavor.

The present study is devoted to the experimental characterization of a new family of swirlers currently being developed in a partnership between PUC-Rio and EM2C/CNRS laboratory at CentraleSupelec (Figueira da Silva *et al.*, 2017). The swirl number is classically defined as the ratio between the axial flux of tangential momentum and the axial momentum flux. The considered radial swirlers are characterized by different feed orifices diameter, number and angle, and also by variations on the central inverted cone bluff-body position. This work is a first step towards a more comprehensive experimental study involving velocity and species measurements.

The present work thus follows several recent numerical studies on lean premixed turbulent swirl stabilized combustion. Using LES, Bourgouin *et al.* (2013) determined how minute vane modification on a radial swirler impacts both the average velocity distribution and the unsteady flow structures, such as the classical precessing vortex core found on such swirling configurations. The unsteady flowfield structure and corresponding flame topologies were shown to be influenced by the combustion chamber wall temperature by Nogenmyr *et al.* (2013), who considered radial swirlers also. Orbay *et al.* (2013) compared experimental and LES isothermal and reactive flowfields results of a radial swirling combustion chamber, with emphasis on the role played by the outlet contraction. Chterev *et al.* (2014) studied axial swirling lean premixed turbulent combustion, comparing the LES velocity fields and flame topologies to those experimentally measured. A dynamic sub-filter model was used to describe the momentum transport, whereas combustion is modeled using an artificially thickened flame approach and a reduced chemistry mechanism. Fluid swirl number measurements by Durox *et al.* (2013) have been shown to exhibit significant discrepancies with respect to the swirl number which may be determined based on a formal order of magnitude analysis from the relevant geometrical features Galley *et al.* (2011).

Amato *et al.* (2011) developed a combustor blow-off model based on the computed adiabatic flame temperature and the associated effect on the extinction strain rate of laminar premixed flames. Even if the fluid dynamics time scale is assumed invariant, the measured blow-off velocity evolution with mixture equivalence ratio is captured by this model. Using a combination of an axial swirler and a bluff-body somewhat similar to the one developed in the present work, Cavaliere *et al.* (2013) demonstrated that a blow-off Damköhler number could be expressed for the different studied

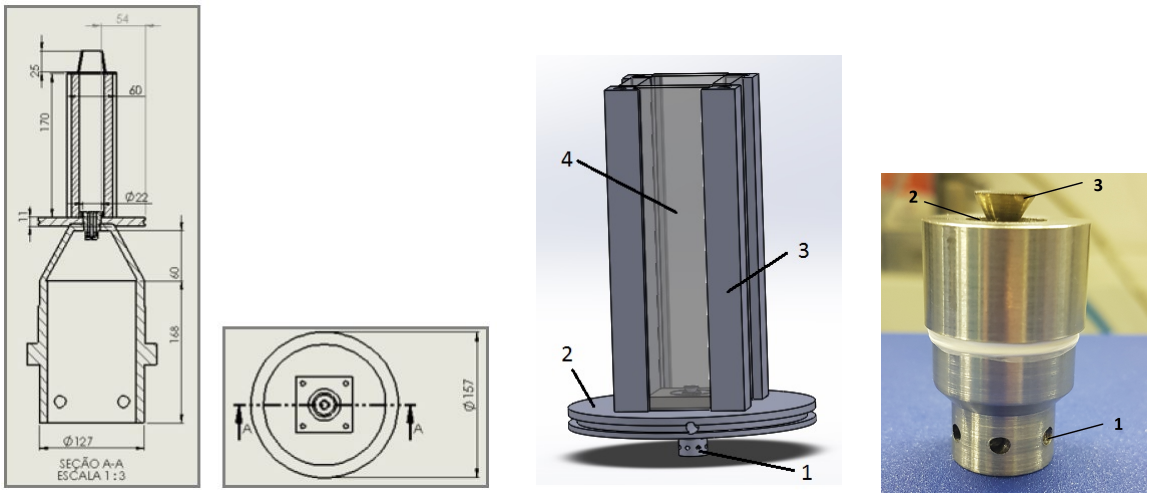

(a) Burner scheme

(b) Combustion Chamber: 1 - swirler, 2 - cooling base, 3 - confinement, 4 - quartz window

(c) Swirler: 1 - air/fuel inlet orifices, 2 - flow outlet area, 3 - bluff-body

Figure 1. Combustion chamber and a typical swirler.

flames as a function of the combustor power. This Damköhler number was defined as the square root of ratio between the bulk flow and the unstretched laminar premixed flame time scales. More recently Jerzak and Ku (2016) evidenced how the natural gas combustion blow-off and flash-back diagrams are influenced both by the swirl number and by the $O_2/N_2/CO_2$ content in the mixture. It has been demonstrated that, for a given total mass flow rate, increasing either the swirl number or the oxygen content allows an ampler operational range, in terms of equivalence ratio or heat input. Combustion chamber geometry has been found to change the methane-air blow-off limit by Tong *et al.* (2016). Indeed, for a given mass flow rate and swirl number, a circular cross section combustor led to smaller blow-off equivalence ratio compared to a rectangular one. Jourdaine *et al.* (2017a) compared premixed turbulent swirling flames of different $O_2/N_2/CO_2$ and CH_4 content, evidencing that the swirl number, the adiabatic flame temperature and the ratio between the flow bulk velocity exert a controlling effect on the flame shape and position. For the studied equivalence ratios and CO_2 dilutions, flame shape transition occurred always at the same swirl number value. Watanabe *et al.* (2016); Taamallah *et al.* (2017a) determined that the mechanisms controlling some of the flame shape transitions are associated to the ratio between a recirculation zone characteristic frequency and the premixed flame extinction strain rate. Furthermore, this frequency has been shown to be Reynolds number independent and to be a linear function of the inlet flow bulk velocity, leading to a constant Strouhal number.

The above cited studies indicate that the different combustion regimes found in turbulent premixed swirling combustors are influenced by the swirl number, the Reynolds number, the mixture composition (via the adiabatic flame temperature), and a Damköhler number. The endeavor of this paper is thus to characterize the influence of a recently proposed (Figueira da Silva *et al.*, 2017) swirler configuration on the boundaries between the observed combustion regimes. This characterization is performed by means of OH^* chemiluminescence and overall flame chemiluminescence.

2. METHODOLOGY

2.1 Combustion chamber and swirlers

Figure 1(b) presents the combustion chamber. The methane/air mixture is introduced through a convergent located upstream to the swirlers (not shown). The combustion chamber is limited by a confinement placed at the top of the convergent section (Fig. 2). The confinement consists of a stainless steel base and four quartz windows of 10 mm thickness and 170 mm height. Cooling water flows through the steel base.

One of the considered swirlers is shown in Fig. 1(c) as a typical example. The gas mixture is fed to the chamber through the orifices which are inclined with respect to the main swirler axis. The orifices are tangent to the 10 mm diameter swirling chamber walls, which length is 33 mm. The central part of this chamber is occupied by a 4 mm diameter cylinder, which is topped by an inverted cone that has a base diameter of 8 mm . This cone base acts as a flame stabilizing bluff-body.

The power of the burner, calculated as $P = \dot{m} \cdot LHV$, where $\dot{m}$ is the mass flow rate and LHV is the lower heating value of methane, and is found to vary between 0.5 and 3.6 kW. The Reynolds number is estimated at two different sections: at the flow inlet (orifices) and at the flow outlet (bluff-body). The characteristic diameter used for calculating Re at the inlet is the orifice diameter, d multiplied by the number of orifices, n. The characteristic diameter of the flow

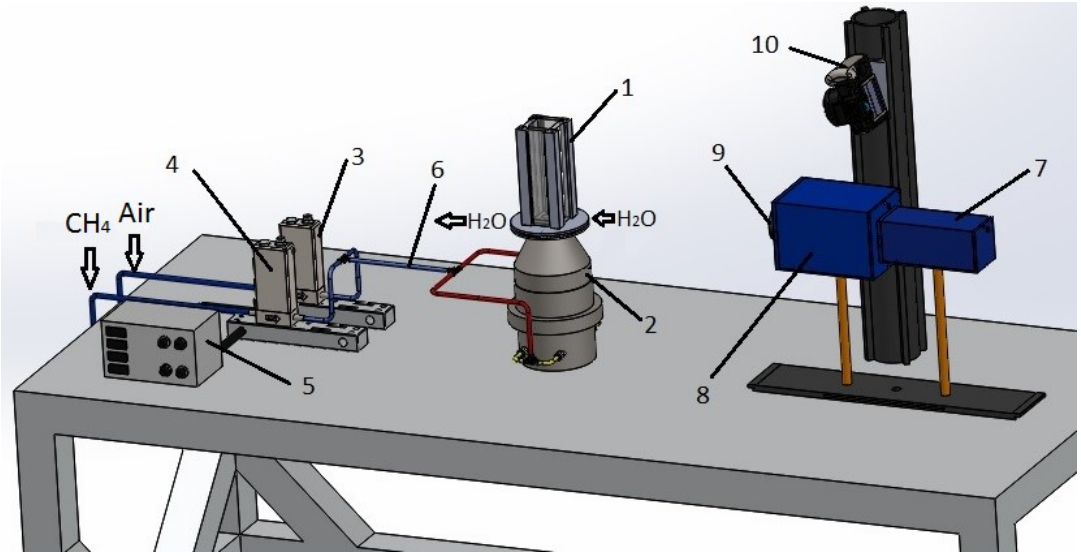

Figure 2. Experimental test bench scheme: 1 - combustion chamber, 2 - convergent, 3 - air flowmeter, 4 - methane flowmeter, 5 - flowmeter controller, 6 - mixture pipe, 7 - CCD camera, 8 - image intensifier IRO, 9 - Canon camera
.

outlet is the hydraulic diameter of the cone trunk of the bluff-body:

$$Re_{in} = \frac{4\dot{\forall}}{\nu n \pi d}; \quad Re_{out} = \frac{4\dot{\forall}}{\nu(D - D_b)}, \tag{1}$$

where ν is the mixture kinematic viscosity, D is the inner diameter of the swirler, D_b is the diameter of the inverted cone base and $\dot{\forall}$ is the flow rate. The corresponding values are determined to span from 2.1×10^3 to 7.4×10^3 (Re_{in}) and from 5.1×10^4 to 1.4×10^5 (Re_{out}).

2.2 Swirl number

The swirl number (S) characterizes the swirl intensity and classically is defined as the ratio between the axial flux of tangential momentum, G_θ, and the axial momentum flux, G_z. Indeed, following Durox *et al.* (2013), assuming that the fluid performs a solid body rotation in the swirler, $u_\theta(r) = \Omega r$, and that the axial velocity component (u_z) is uniform and ignoring the pressure effects, the swirl number is expressed as:

$$S = \frac{G_\theta}{RG_z} = \frac{\int_0^R u_z u_\theta r^2 dr}{R\int_0^R u_z^2 r dr} = \frac{1}{2}\frac{u_\theta(R)}{u_z}, \tag{2}$$

where R is the swirler radius.

Considering the mass conservation in the tubes and the geometry of the exit section shown in Fig. 3, it is possible to determine $u_\theta(R)$ as

$$u_\theta = \dot{\forall}\frac{4}{\pi n d^2}\sin\theta, \tag{3}$$

where $\sin\theta = \frac{l}{D/2}$.

To determine u_z, it is assumed that the velocity vector is parallel to inverted cone surface at the exit plan. Considering the geometry shown in Fig. 3, volume flux at this plan allows to write

$$\dot{\forall} = u_z A_z \left(1 + \frac{\tan\beta}{\tan\alpha}\right). \tag{4}$$

$$\tan\beta = \frac{D_b - D_i}{2h_b}; \quad \tan\alpha = \frac{D - D_b}{2h_i}. \tag{5}$$

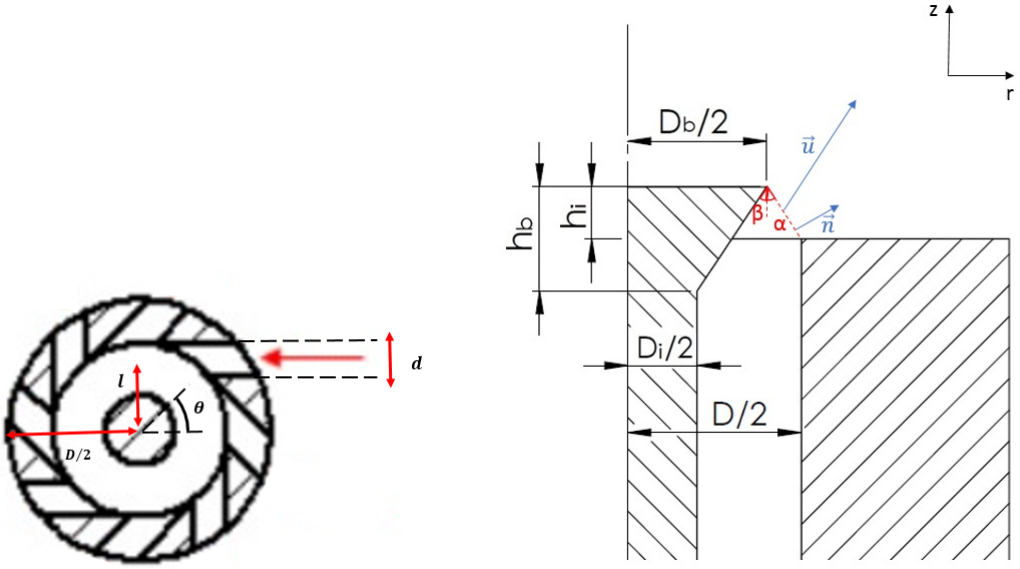

Figure 3. Swirler intlet (letf) and exit (right) plans.

where D_i is the diameter of the inner cylinder, h_i is the clearance between the bluff-body top surface and the swirler exit and h_b is the height of the inverted cone base. Replacing these expressions in Eq. (5) one can write

$$\frac{1}{u_z} = \frac{\pi D^2}{4\dot{\forall}} \left[1 - \frac{D_b}{D}^2\right] \left[1 + \frac{D_b - D_i}{D - D_b} \frac{h_i}{h_b}\right]. \tag{6}$$

Finally, the swirl number can be expressed as

$$S = \underbrace{\frac{lD}{nd^2}}_{(a)} \underbrace{\left[1 - \left(\frac{D_b}{D}\right)^2\right]}_{(b)} \underbrace{\left[1 + \frac{D_b - D_i}{D - D_b} \frac{h_i}{h_b}\right]}_{(c)}. \tag{7}$$

Equation (7) represents the combination of the usual swirl number expression (a), the influence of the central cylinder (b) and the combined effect of the bluff-body angle and height (c), showing how the geometry of the swirler influences the swirl number.

In order to analyze different regions of confined flames, a preliminary study was made using two swirlers, SW08 and SW05. SW08 is shown in Fig. 1(b). The main difference between them is the flow inlet section. Indeed, SW05 has only 5 orifices, each with 2.5 mm diameter, therefore 24.54 mm^2 of inlet area. SW08 has 8 orifices, each with 2.0 mm, so its area is 25.13 mm^2, i.e., slightly higher than SW05. Both swirlers have the same bluff-body type and dimensions.

The final version of the manuscript will include analysis of the influence of different geometrical parameters on the Swirl number and, thus, on the obtained flow regimes.

2.3 Experimental setup

Figure 2 shows the experimental test bench which is composed of the burner, the combustion chamber, the convergent, two flow meters (methane and air), a flow controller, a CCD camera with an intensifier and a Canon camera.

The flow meter used for methane is a Bronkhorst mass flow controller (series F-201AC) with a maximum range of 138.9 cm^3/s with 0.5 % reading plus 0.1 % full scale uncertainty. The air volumetric flow rate is measured using a pair of rotameters (Omega, 4T70903X12 and 4T708TX12 models), with a 2 % reading plus 2 % full scale uncertainty and maximum range of 1 dm^3/s. A type T thermocouple (Salvi Casagrande) is used to measure the air flow temperature. In this study, the CH_4 flow rate varies from 18.6 cm^3/s to 107.2 cm^3/s and the total volumetric flow rate varies from 441.1 cm^3/s to 1146.1 cm^3/s, thus leading to large variations of equivalence ratio, between 0.44 and 1.14.

2.4 Flame imaging

In order to characterize the overall flame topologies, time-integrated chemiluminescence images of the combustion process have been obtained by using a Canon EOS Rebel TS camera, equipped with a 58 mm diameter lens, but no filters.

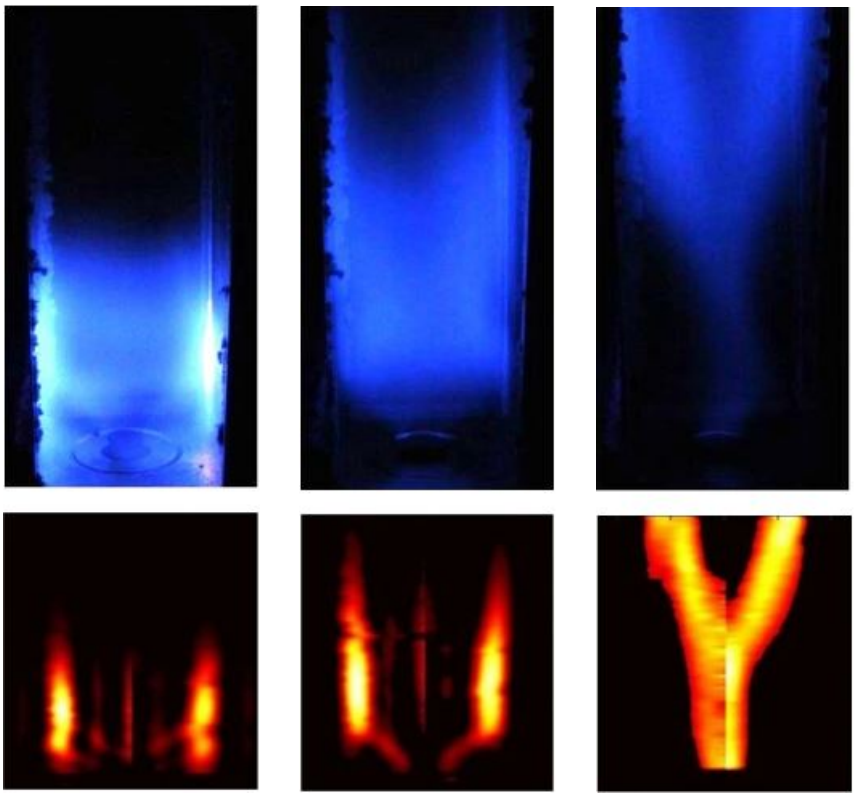

(a) $\phi = 1.12$, $\dot{\forall} = 1150$ cm^3/s (b) $\phi = 0.95$, $\dot{\forall} = 1133$ cm^3/s (c) $\phi = 0.84$, $\dot{\forall} = 1122$ cm^3/s

Figure 4. Flame topologies for different equivalence ratios (ϕ) and mixture flowrate ($\dot{\forall}$), SW08: direct photos (top), deconvoluted OH* images (bottom).

All images presented in this study used $f-36$ aperture and exposure time of 500 ms.

A LaVision Imager Intense CCD (Charge Coupled Device) camera has been used to record flame images with an exposure time of 4 ms and $f-8$ aperture. Furthermore, a LaVision image intensifier IRO (Intensified relay-optics), equipped with a 310 nm filter, 100 % gain and gate of 100 ms was used. These chemiluminescence images are classically associated with the OH* radicals and, thus to the premixed flame front.

The OH* images have been deconvoluted by employing an Abel inversion technique which uses a Fourier-based algorithm (Pretzier, 1991; Pretzier *et al.*, 1992). The inversion process transforms the images obtained along the line of sight into a cross-sectional representation, assuming axial symmetry. For a given image, its centroid is first determined, then the deconvolution of the left and right positions is performed. In this study, 16 modes of the Fourier expansion have been used. One should note that this inversion technique is valid when axial symmetry hypothesis may hold, which is evidently not the case of the present square cross section combustion chamber. Nevertheless, the Abel-inverted OH* images are used to roughly evidence the location and shape of the average flame front.

3. RESULTS AND DISCUSSION

In this section, the flame topologies observed for each specific operating condition are first presented. The used topology classification follows that proposed by Shanbhogue *et al.* (2016), since it is possibly the one that most closely describe the observed phenomena. The corresponding stability maps of the combustion for this experimental setup are then discussed.

3.1 Flame topologies

Three direct photos of confined flames at different combustion regimes, using the SW08 swirler are shown in Fig. 4. The swirl number computed with Eq. (7) is $S = 1.4$. All pictures have been taken with a fixed air flow rate of 1039 cm^3/s, whereas the methane varies from 83 to 111 cm^3/s. These pictures allow to verify that the flame stabilizes in three different shapes: Recirculating Zone (RZ), V and Tornado, from left to right. The images on the second row show deconvoluted OH* pictures of the average flames, obtained through the use of Abel's inversion, as studied by Figueira da Silva *et al.* (2017). Again, each image has been obtained in the different stable regions (RZ, V and Tornado).

In Fig. 4(a) it may be assumed that a recirculating zone exists, as observed by Shanbhogue *et al.* (2016); Guiberti *et al.* (2015), given the structure of the flow. Such recirculating zone flames, known as flame type IV, are observed for rich fuel/air mixtures and exhibit an important interaction with the combustion chamber walls. Indeed, this figure shows that the regions with highest luminous intensity are located along the walls of the combustion chamber.

The center picture, Fig. 4(b), presents a slightly different behavior: the flame is anchored only at the swirler bluff-body. It has a V-shape (known as flame type III) and it's possible to observe that the regions with highest luminous intensity are also located at the walls of the confinement, so the flame presents a strong interaction with the walls, as is the case of flame type IV. At the used flow rates, this V-shape is found to occur for flow rates close to stoichiometry.

The rightmost image, Fig. 4(c), shows a flame that is found close to the blow-off limit. It has a tornado shape and does not interact with the walls, and is also known as flame type I. Analyzing the inverted image of the tornado flame it is possible to conclude that the flame is uncoupled from the swirler and there is a flame surface bifurcation, which means there is a higher concentration of OH* in the lateral of the combustion chamber. It is important to highlight that there is a flame instability zone between each stable flame type shown, which will be discussed in section 3.2

Flame topologies are controlled by the mixture composition, flow rate and swirl number. Changes in the flame shape are related with the equivalence ratio of the mixture and acoustic instabilities, as evidenced by Shanbhogue *et al.* (2016), which suggest that:

- Shape and macro structure of the flame are related to the equivalence ratio of the mixture (when Re is constant) and significant changes are observed when critical values of fuel concentration are crossed;
- The velocity of the flow varies as the equivalence ratio changes, in other words, there is an exclusive flow associated with each flame shape;
- When the equivalence ratio increases, the burning zone becomes shorter and tends to stay closer to the swirler.

It is important to highlight that premixed flames have a huge impact on the flow dynamics. This is due to the volumetric expansion over the flow path during combustion actually occurs.

3.2 Operation regimes diagram

In order to compare the influence of the swirl number on combustion regimes, another type of bluff-body has been developed for the swirler SW08. The bluff-body height is the same as the swirler surface, $h_i = 0$, therefore, a difference between those swirlers is the outlet area. The results obtained with both swirlers are compared here. To this end, the same operating conditions have been considered.

Figures 5 and 6 give diagrams where the boundaries between the combustion regimes (flame topologies) are plotted for the the swirler whose bluff-body height is $h_i = 3$ mm and for the one whose bluff-body height is the same as the swirler surface, $h_i = 0$, respectively. This diagram shows these boundaries as a function of the mixture flow rate and fuel/air equivalence ratio.

The tests have been carried out by fixing the air flow rate and progressively decreasing the methane flow rate. The air flow rates studied range from 393 to 1039 cm^3/s. In this figure, the experimentally determined regime borders are given by the symbols, each symbol corresponding to a particular regime border. It is important to highlight that the limits between each regime have been defined visually, and repeatedly observed to occur at the depicted symbols positions. Least squares fits of these regimes borders are also given.

Following Shanbhogue *et al.* (2016), six distinct regimes have been identified, among which are the three stable ones presented in the previous section. The results shown in Fig. 5 will be discussed starting from a high equivalence ratio value and progressively diminishing its value. In region IV, the flame is stabilized in the RZ, as shown in Fig. 4(a). Upon decreasing the equivalence ratio, when the boundary is reached, the flame goes through an instability zone, IVf, where it flickers and presents a distinct acoustic tone. This seems to occur because of the intermittent presence of the flame in the recirculation, as discussed by Shanbhogue *et al.* (2016). Once the border between regions IVf and III is crossed, the flame is again stable and a corresponding representative average flame picture in this may be seen in Fig. 4(b). Indeed, the flame presents a V-shape until it reaches another instability border and moves to region II. This region presents a particular characteristic behavior: for small flows rates, extinction occurs (which is represented by open symbols). However, for larger flows rates (represented by solid symbols) combustion instability is observed. This second type of instability seems to be related to a large-scale, lower frequency pulsations of the combustion chamber. Further decreasing the equivalence ratio leads to region I, which corresponding flame structure can be observed in Fig. 4(c). By decreasing the equivalence ratio the blow-off limit is reached, which means that in the region below the pink border there is no flame within the combustor.

The swirl number computed with Eq. (7) for the swirler whose bluff-body height is the same as the swirler surface is 0.9. For SW08 with $S = 1.4$ the stability zones IV and III are larger when compared to the swirler whose bluff-body height is the same as the swirler surface, with $S = 0.9$. However, for the stable regime I, the stability range is larger

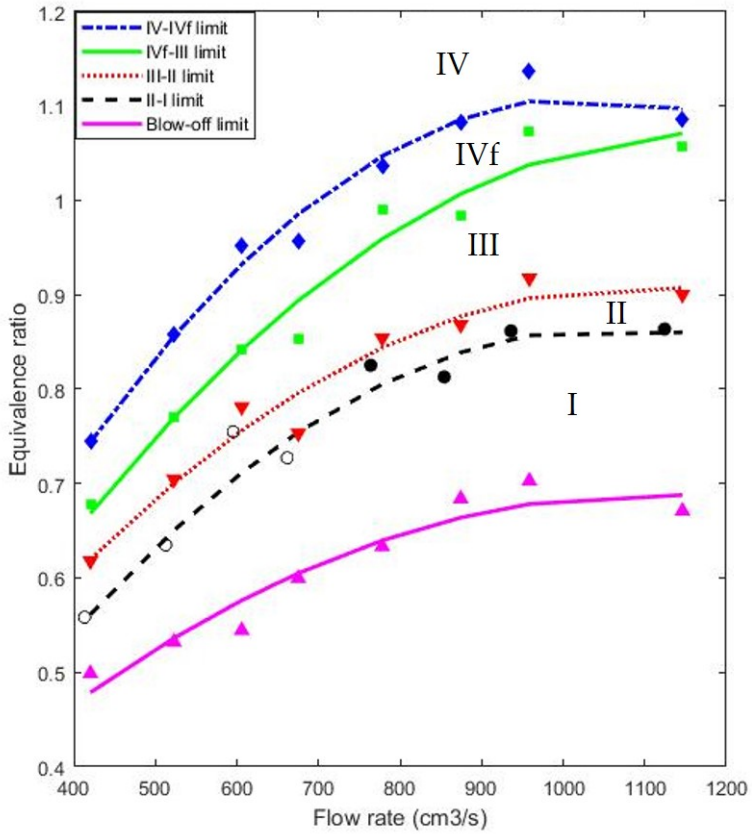

Figure 5. **Operation Regime diagram, S=1.4** - IV Stability: RZ flame, IVf Instability, III Stability: V flame, II Instability, I Stability: tornado flame. Flame blow-off occurs at the lowermost line.

when $S = 0.9$, in which case the blow-off occurs at a lower equivalence ratio. When S = 0.9 the boundaries are shifted downward, which means that it is possible to achieve the same regime with lower equivalence ratio, and thus using less fuel. It should be noted that stable flame regimes are not altered by the swirl number. However, the position of the diagram (flow $\times$ equivalence ratio) where each regime is observed varies, as seen above.

Recently, several studies have attempted to unveil the underlying mechanisms that control the separation between those different combustion regimes. The experimental work of Taamallah *et al.* (2015) has determined the role of the combustor length and H_2 addition on the onset frequencies of the thermo-acoustic instabilities characteristic frequencies. Even though changing the combustor length has not been attempted here, such a characteristic frequency analysis will be the subject of future work. Taamallah *et al.* (2017b) demonstrated that the boundary between regions III and IV is controlled by the flow bulk velocity and that the flame Strouhal number at the outer recirculation zone is Reynolds number independent. The role of the computed premixed flame extinction strain rate on the outer recirculation zone flame frequency has also been demonstrated. Since similar regimes have been observed here, it could be anticipated that a similar scaling hold, which is currently being examined. Jourdaine *et al.* (2017b) have determined that, at a given equivalence ratio, the lifted flame leading edge position is independent of: (i) the ratio between the flow bulk velocity and the premixed flame speed and (ii) the adiabatic flame temperature of the combustible mixture. Such a verification of independence could also have been performed here, in order to evidence the possible influence on the flame blow-off boundary displacement observed.

4. CONCLUSIONS AND PERSPECTIVES

- A novel radial swirler geometry featuring a central bluff-body has been developed that allows to control the swirl number by changing the bluff-body height only;
- A first characterization of different combustion regime/flame topologies identified the stability boundaries as a function of fuel and air flow rates for two swirlers having different swirl numbers;
- Identical combustion regimes have been observed for those two swirlers, which are analogous to those found in the

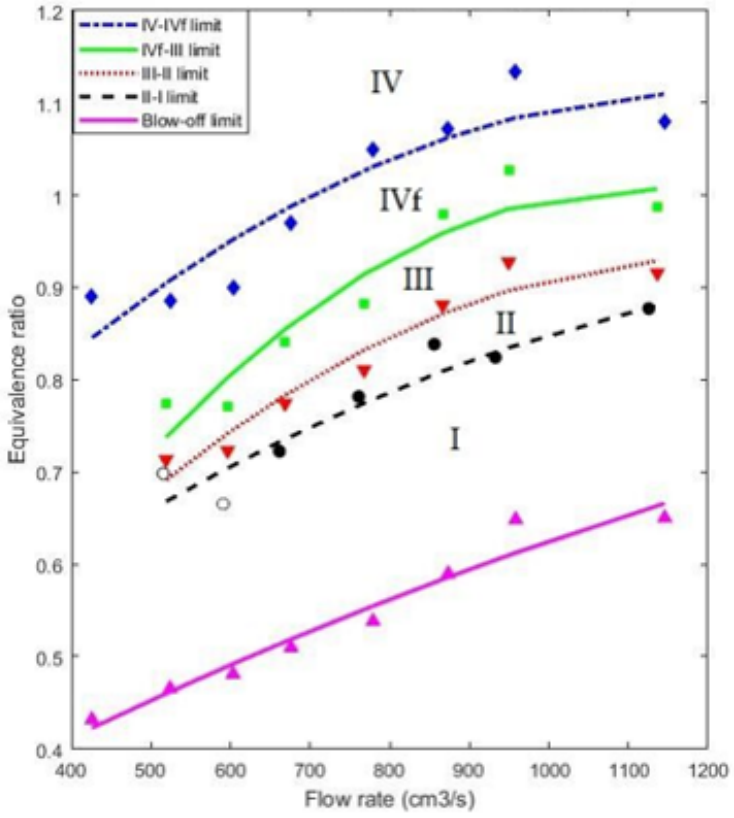

Figure 6. **Operation Regime diagram, S=0.9** - IV Stability: RZ flame, IVf Instability, III Stability: V flame, II Instability, I Stability: tornado flame. Flame blow-off occurs at the lowermost line.

literature, and that involve both stable or unstable combustion;

- The swirl number has been shown to influence the boundary between those combustion regimes. Indeed, the larger swirl number studied, $S = 1.4$, led to a larger extend of stable regime III, which is a regime of practical relevance to gas turbines. However, the blow-off limit for such a swirler occurs for a larger value of equivalence ratio, which is not interesting to propulsion applications;
- Future work will involve a characterization of flame surface density by means of OH-PLIF, in order to support modeling efforts;
- This combustion chamber will also be adapted to burn gaseous ethanol/butanol/air mixtures, thus allowing to investigate the corresponding combustion regimes changes.

5. ACKNOWLEDGEMENTS

This work was supported by PUC-Rio and Laboratoire EM2C CNRS, CentraleSupelec (France). L.F. Figueira da Silva was on leave from the Institut Prime (CNRS, France), L.C. Piton and G.S. Nobrega had scholarships from CNPq (Brazil). The authors gratefully acknowledge the support for the present research provided by Conselho Nacional de Desenvolvimento Científico e Tecnológico, CNPq, under the Research Grants No. 306069/2015-6 and 403904/2016-1.

6. REFERENCES

Amato, A., Hudak, B., D'Carlo, P., Noble, D., Scarborough, D., Seitzman, J. and Lieuwen, T., 2011. "Methane oxy-combustion for low CO_2 cycles: Blowoff measurements and analysis". *Journal of Engineering for Gas Turbines and Power*, Vol. 133, pp. 1–9.

Bourgouin, J., Moeck, J., Durox, D., Schuller, T. and Candel, S., 2013. "Sensitivity of swirling flows to small changes in the swirler geometry". *Comptes Rendus Mecanique*, Vol. 341, pp. 211–219.

Candel, S., Durox, D., Schuller, T., Bourgouin, J. and Moeck, J., 2014. "Dynamics of swirling flames". *Annual Review of Fluid Mechanics*, Vol. 46, pp. 147–173.

Cavaliere, D.E., Kariuki, J., Mastorakos, E., Cavaliere, D.E., Kariuki, J. and Mastorakos, E., 2013. "A comparison of the blow-off behaviour of swirl-stabilized premixed, non-premixed and spray flames". *Flow, Turbulence and Combustion*, Vol. 91, pp. 347–372.

Chterev, I., Foley, C., Foti, D., Kostka, S., Caswell, A., Jiang, N., Lynch, A., Noble, D., Menon, S., Seitzman, J. and Lieuwen, T., 2014. "Flame and flow topologies in an annular swirling flow". *Combustion Science and Technology*, Vol. 186, pp. 1041–1074.

Durox, D., Moeck, J., Bourgouin, J., Morenton, P., Viallon, M., Schulle, T. and Candel, S., 2013. "Flame dynamics of a variable swirl number system and instability control". *Combustion and Flame*, Vol. 160, pp. 1729–1742.

Figueira da Silva, L., Mergulhão, C., Piton, L., Scouflaire, P. and Darabiha, N., 2017. "Experimental study of a lean premixed turbulent swirling flame stabilization". *24th ABCM International Congress of Mechanical Engineering*.

Galley, D., Ducruix, S., Lacas, F. and Veynante, D., 2011. "Mixing and stabilization study of a partially premixed swirling flame using laser induced fluorescence". *Combustion and Flame*, Vol. 158, pp. 155–171.

Guiberti, T., Durox, D., Zimmer, L. and Schuller, T., 2015. "Analysis of topology transitions of swirl flames interacting with the combustor side wall". *Combustion and Flame*, Vol. 162, pp. 4342–4357.

Huang, Y. and Yang, V., 2009. "Dynamics and stability of lean-premixed swirl-stabilized combustion". *Progress in Energy and Combustion Science*, Vol. 35, pp. 293–364.

Jerzak, W. and Ku, M., 2016. "Experimental study of impact of swirl number as well as oxygen and carbon dioxide content in natural gas combustion air on flame flashback and blow-off". *Journal of Natural Gas Science and Engineering*, Vol. 29, pp. 46–54.

Jourdaine, P., Mirat, C., Caudal, J., Lo, A. and Schuller, T., 2017a. "A comparison between the stabilization of premixed swirling CO_2- diluted methane oxy-flames and methane/air flames". *Fuel*, Vol. 201, pp. 156–164.

Jourdaine, P., Mirat, C., Caudal, J., Lo, A. and Schuller, T., 2017b. "A comparison between the stabilization of premixed swirling co2-diluted methane oxy-flames and methane/air flames". *Fuel*, Vol. 201, pp. 156 – 164.

Nogenmyr, K., Cao, H., C.K., C. and Cheng, R.K., 2013. "Effects of confinement on premixed turbulent swirling flame using large eddy simulation". *Combustion Theory and Modelling*, Vol. 17, pp. 1003–1019.

Orbay, R., Nogenmyr, K., Klingmann, J. and Bai, X., 2013. "Swirling turbulent flows in a combustion chamber with and without heat release". *Fuel*, Vol. 104, pp. 133–146.

Pretzier, G.A., 1991. "A new method for numerical abel-inversionl". *Zeitschrift für Naturforschung*, Vol. 46, pp. 639–641.

Pretzier, G.A., Jäger, H., Neger, T., Philipp, H. and Woisetschläger, J., 1992. "Comparison of different methods of abel inversion using computer simulated and experimental side-on data". *Zeitschrift für Naturforschung*, Vol. 47a, pp. 639–641.

Shanbhogue, S., Sanusi, Y., Taamallah, S., Habib, M., Mokheimer, E. and Ghoniem, A., 2016. "Flame macrostructures, combustion instability and extinction strain scaling in swirl-stabilized premixed CH_4/H_2 combustion". *Combustion and Flame*, Vol. 163, pp. 494–507.

Taamallah, S., Chakroun, N.W., Watanabe, H., Shanbhogue, S.J. and Ghoniem, A.F., 2017a. "On the characteristic flow and flame times for scaling oxy and air flame stabilization modes in premixed swirl combustion". *Proceedings of the Combustion Institute*, Vol. 36, No. 3, pp. 3799–3807.

Taamallah, S., Chakroun, N.W., Watanabe, H., Shanbhogue, S.J. and Ghoniem, A.F., 2017b. "On the characteristic flow and flame times for scaling oxy and air flame stabilization modes in premixed swirl combustion". *Proceedings of the Combustion Institute*, Vol. 36, No. 3, pp. 3799 – 3807.

Taamallah, S., LaBry, Z.A., Shanbhogue, S.J. and Ghoniem, A.F., 2015. "Thermo-acoustic instabilities in lean premixed swirl-stabilized combustion and their link to acoustically coupled and decoupled flame macrostructures". *Proceedings of the Combustion Institute*, Vol. 35, No. 3, pp. 3273 – 3282.

Tong, Y., Li, M. and Jens, K., 2016. "Influence of combustor geometry on swirl stabilized premixed methane-air flame". In *Proceedings of ASME Turbo Expo 2016: Turbomachinery Technical Conference and Exposition*. pp. 1–10.

Watanabe, H., Shanbhogue, S.J., Taamallah, S., Chakroun, N.W. and Ghoniem, A.F., 2016. "The structure of swirl-stabilized turbulent premixed CH_4/air and CH_4/O_2/CO_2 flames and mechanisms of intense burning of oxy-flames". *Combustion and Flame*, Vol. 174, pp. 111–119.

7. RESPONSIBILITY NOTICE

The authors are the only responsible for the printed material included in this paper.